

Size-dependent effects on equilibrium stress and strain in nickel nanowires

Yuhua Wen,* Yang Zhang, and Zizhong Zhu

Department of Physics, and Institute of Theoretical Physics and Astrophysics, Xiamen University, Xiamen 361005, People's Republic of China

(Received 17 April 2007; revised manuscript received 1 July 2007; published 19 September 2007)

Using molecular static calculations with the quantum corrected Sutton-Chen-type many-body potential, we have studied the stress and strain characteristics in nickel nanowires along [100], [110], and [111] crystallographic orientations under the equilibrium state. The main focus of this work is the size-dependent effects on these characteristics above. We deduce from the common neighbor analysis that surface region approximately consists of two layer atoms. Further, we extract the equilibrium characteristics in both surface and core regions of nanowires. The results show that with increasing diameter, the equilibrium stress and strain which are compressive decrease sharply in the core region, while the surface tensile stress starts to increase, and gradually trends to a nonzero constant. Due to much larger compressive stress and smaller modulus, the core of [100] nanowire endures larger compressive strain than that of [110] and [111] nanowires.

DOI: 10.1103/PhysRevB.76.125423

PACS number(s): 68.65.La, 62.25.+g, 81.07.Bc

I. INTRODUCTION

As one of the most important one-dimensional (1D) nanostructures, nanowires (NWs) have attracted a great deal of interests due to their pivotal role in future electronic, optoelectronic, and nanoelectromechanical systems.^{1,2} With decreasing characteristic dimensions to nanoscale level, the wires are formed by a reduced number of atoms and the majority of them are located at the surface. This may lead to different behaviors when compared to their macroscopic counterpart and result in strong size effects.³⁻⁷

It is of vital importance for us to understand the mechanical properties of nanowires for better control of their fabrication and functionality. However, characterization of these properties is a challenge to many existing testing and measuring techniques because of the tiny dimension of nanowires making the manipulation rather difficult.^{8,9} To date, some experimental measurements, such as scanning electron microscopy, transmission electron microscopy, and atomic force microscopy focus on the bending tests to investigate the mechanical responses of Ag, Pb, Au, Si, SiC, and ZnO nanowires, which have been deduced to different results.^{3-6,10,11} For example, some experiments show that nanowire's Young's moduli decrease dramatically with decreasing diameters,^{3,4} whereas others show an opposite tendency.^{5,6} Especially for SiC and Au NWs, their Young's moduli are essentially independent of diameter.^{10,11} Atomistic computer simulations, usually using semiempirical or empirical approaches to describe interatomic interactions, are an alternative way to understand the mechanical behavior of nanowires.¹²⁻²¹ These simulations show that size effects¹⁴⁻¹⁶ and nonlinear effects¹⁷ play an important role in determining their properties.

Although there have been many theoretical, experimental, and computational studies dedicated to explore and explain the mechanical response of nanowires, the stress and strain characteristics of nanowires under the equilibrium state are easily omitted by researchers. Generally, these characteristics are essentially size dependent and crucial for understanding the structural evolution and the mechanical behavior of

nanowires. For example, the surface stress can drive the reorientation of nanowires,¹⁸⁻²⁰ and further affect their structural stability and properties.¹⁴⁻²¹ So, in this paper, we will employ molecular static simulations to investigate the equilibrium stress and strain of nanowires, and address the size-dependent effects on their characteristics. A brief description of the computational methods is given in the following section. We present the calculated results, discussion, and comparisons with other results in the third section. The main conclusions are summarized in the fourth section.

II. COMPUTATIONAL METHODS

In molecular static calculations, we use the quantum corrected Sutton-Chen (Q-SC)-type potentials modified by Kimura *et al.*²² to describe interatomic interactions for metal nanowires. These potentials represent many-body interactions, and their parameters are optimized to describe the lattice parameter, cohesive energy, bulk modulus, elastic constants, phonon dispersion, vacancy formation energy, and surface energy, leading to an accurate description of many properties of metals and their alloys.²³⁻²⁵ For the SC-type force field, the total potential energy for a system of atoms can be written as

$$U = \sum_i U_i = \sum_i \varepsilon \left[\frac{1}{2} \sum_{j \neq i}^N V(R_{ij}) - c \sqrt{\rho_i} \right]. \quad (1)$$

Here $V(R_{ij})$ is a pair interaction function defined by the following equation:

$$V(R_{ij}) = \left(\frac{a}{R_{ij}} \right)^n, \quad (2)$$

accounting for the repulsion between the i and j atomic cores; ρ_i is a local electron density accounting for cohesion associated with atom i defined by

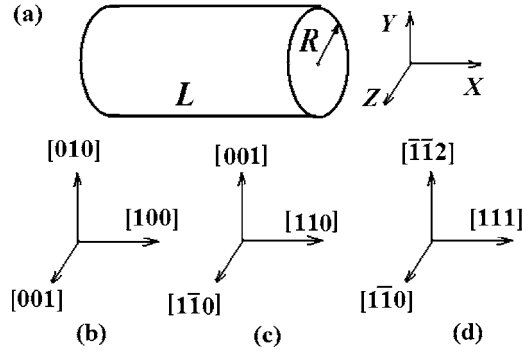


FIG. 1. Schematic illustration of the simulation cell used to study the equilibrium characteristics of nanowires. The X axis is the axial direction and is subjected to periodic boundary conditions, while the surface is free. (b)–(d) illustrate the crystallographic directions of nickel nanowires. L and R denote the length and radius of the computational cell, respectively.

$$\rho_i = \sum_{j \neq i}^N \phi(R_{ij}) = \sum_{j \neq i}^N \left(\frac{a}{R_{ij}} \right)^m. \quad (3)$$

In Eqs. (1)–(3), R_{ij} is the distance between atoms i and j , a is a length parameter scaling all spacings (leading to dimensionless V and ρ), and c is a dimensionless parameter scaling the attractive terms, ε sets the overall energy scale, and n and m are the integer parameters such that $n > m$. Given the exponents (n, m) , c is determined by the equilibrium lattice parameter, and ε is determined by the total cohesive energy. For the Q-SC-type potential of Ni, the parameters are given as follows: $n=10$, $m=5$, $\varepsilon=7.3767$ meV, $c=84.745$, and $a=3.5157$ Å.

Circle-cross-section Ni nanowires with diameter ranging from 1.76 to 17.23 nm are constructed from a large cubic fcc single crystal of nickel using certain cylindrical cutoff radii centered at a cubic interstitial site, in which the crystallographic orientations are shown in Fig. 1. In the Y and Z directions, the Ni nanowire spans a finite number of unit cells, while in the X direction, an infinite wire was obtained by applying the periodic boundary condition. Three types of nanowires, i.e., [100], [110], and [111] nanowires, are considered in the present study.

We have performed molecular static simulations to relax fully these nanowires to a local minimum energy state using the conjugate gradient method.²⁶ After the initial relaxation, the nanowires are under the equilibrium state without any external force so that the average stress over the cross section is zero. The stress tensor in nanowire system can be defined²⁷ as

$$\bar{\sigma}_{\alpha\beta} = \frac{1}{V} \left\{ \sum_{i=1}^N m_i v_i^\alpha v_i^\beta + \sum_{i=1}^N \sum_{j>i}^N F_{ij}^\alpha R_{ij}^\beta \right\}, \quad (4)$$

where V and N are the volume and total atomic number of the system, m_i and v_i are the mass and velocity of the i th atom, and F_{ij} and R_{ij} are the force and distance between atoms i and j . The first summation in Eq. (4) is zero at absolute zero temperature. The normal stresses, usually cal-

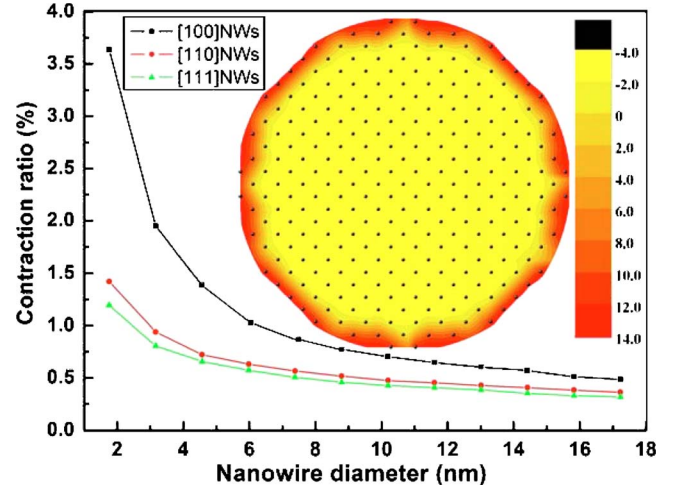


FIG. 2. (Color online) The contraction ratio of nanowire's length along the X direction after the initial relaxation for three nanowires. (inset) The distribution of the normal stress (GPa) along the axial direction in [100] nanowire with 4.56 nm diameter. The positive indicates the tensile stress, while the negative the compressive stress. Black point represents the position of atom in this nanowire.

culated from this equation under unstrained and strained states, are substantially equivalent to that obtained from the first-order derivative of the total energy with respect to strain ε .²¹ The atomic-level stress sensor associated with the i th atom is calculated^{28,29} by

$$\sigma_{\alpha\beta} = \frac{1}{\Omega_i} \left\{ \frac{1}{2} \sum_{j=1(j \neq i)}^N F_{ij}^\alpha R_{ij}^\beta \right\}, \quad (5)$$

where Ω_i is the local volume which can be identified with the volume of the Voronoi polyhedra³⁰ constructed by the perpendicular planes that bisect the lines between atom i and all its neighbor atoms. However, this method of calculating Ω_i is time consuming, so Srolovitz *et al.*³¹ has obtained a sphere whose volume is equal to the original Voronoi volume by the following formulation:

$$\Omega_i = \frac{4}{3} \pi a_i^3, \quad a_i = \frac{\sum_{j \neq i} R_{ij}^{-1}}{2 \sum_{j \neq i} R_{ij}^{-2}}, \quad (6)$$

where a_i is the average radius of atom i , and R_{ij} is the distance between atoms i and its neighbor atom j . In this paper, we also use this formulation to calculate the atomic volume.

III. RESULTS AND DISCUSSION

The results of our simulations will be presented here. Figure 2 shows the contraction ratio of length as a function of the diameter ranging from 1.76 to 17.23 nm for [100], [110], and [111] nanowires under the equilibrium state. For each of three nanowires, the contraction ratio increases with decreasing diameter. This trend is much more remarkable for [100] nanowire than others. The contraction behavior indicates the presence of surface tensile stress. In order to display the

stress distribution in nanowire system, we calculate the normal stress along the axial direction in Y - Z cross section of 4.56 nm diameter [100] nanowire according to Eq. (5), and then illustrate its distribution in Fig. 2 (see inset picture). It can be seen that the stress is tensile in surface region while compressive in interior region. The stress changes from -3.5 GPa in the center to 13.4 GPa in the outermost layer, but it is approximately uniform within a circular region of 1.8 nm radius. This kind of stress distribution is quite similar to that in [110] and [111] nanowires. The nonzero stress indicates that there are residual strains in nanowire after the initial relaxation. That is to say, the surface endures the tensile strain while the interior endures the compressive strain, even if this nanowire is under the equilibrium state.

In order to investigate the size-dependent effects, it is necessary to divide the cross section into interior and surface regions. However, there is no absolute physical boundary between these two regions because it is a gradual process from center layer to outmost layer. For research convenience and simplification of the problem, we use the common neighbor analysis³² (CNA) to analyze the local order in nanowire and determine whether or not an atom belongs to surface region. This analysis assigns four indices $ijkl$ to each pair of atoms, which have common neighbors, and provides a description of the local environment of the pair.^{33,34} Firstly, those pairs of atoms which are separated by less than a physically reasonable cutoff distance are designated nearest neighbors. We use the first minimum in the radial distribution function of the nanowire for the particular pair of atoms as the cutoff distance. For those pairs of atoms which are nearest neighbors i is assigned the value 1. For those pairs of atoms which are not nearest neighbors but which have common neighbors i is assigned the value 2. The index j specifies the number of neighbors common to both atoms. The index k specifies the number of nearest-neighbor bonds between the common neighbors. The index l is needed to differentiate between the cases when the first three indices are the same but the bond geometries are different.

Because the different types of pairs are associated with different types of the local order, the local crystal structure can be determined by investigating the bonds between the neighboring atoms to the atom under investigation. All bonded pairs in the fcc crystal are of type 1421, while the hcp crystal has equal numbers of types 1421 and 1422. We have calculated CNA indices in a number of atomic configurations extracted from molecular static calculations. Considering that pairs beside types of 1421 and 1422 cannot reveal some useful information for fcc metallic nanowire, we have classified all atoms into three categories. Atoms in a local fcc order are considered to be inside the nanowire; atoms in a local hcp order are classified as stacking faults. Atoms in all other local orders are considered to be part of surface. The CNA methods have been successfully used to analyze the structural evolution during the deformation and melting process.³⁵⁻³⁷

Figure 3 illustrates the dependence of the surface volume to bulk ratio on the diameter for [100], [110], and [111] nanowires. As expected, this ratio increases with decreasing nanowire diameter. When the diameter of [100] nanowire is reduced to 1.76 nm, this ratio rises up steeply to 0.449,

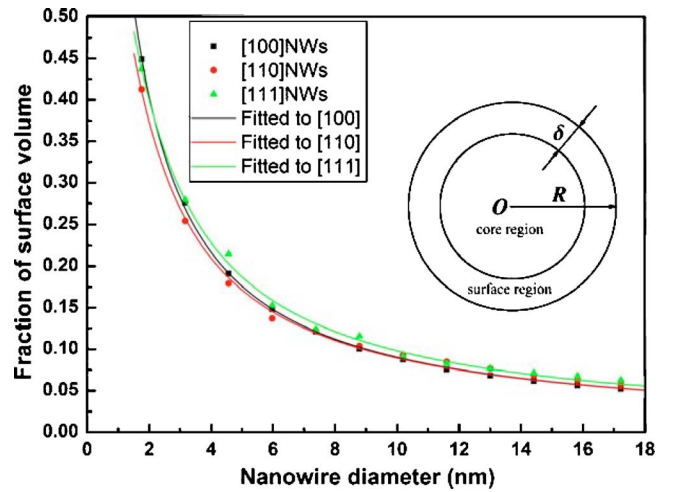


FIG. 3. (Color online) The fraction of surface volume as a function of diameter after the initial relaxation for three nanowires. The discrete points are calculated through the CNA methods; the curves are fitted to these points using Eq. (7). (inset) Schematic illustration of the core-surface composite NW model. R and δ are the radius and surface thickness of nanowire, respectively.

which means that almost 44% of the atoms are situated in the surface region. For [110] and [111] nanowires with the same diameter, the surface volume ratios are 0.413 and 0.437, respectively. The difference of this ratio among the three nanowires is small (below 0.036). If the surface thickness is considered to be a constant δ (see inset picture of Fig. 3), the surface volume ratio can be expressed as the formulation: $f(D) = 4\delta/D - 4\delta^2/D^2$ in terms of theory of continuum media matter (D is the nanowire diameter). Due to the fact of a nanowire consisting of many discrete atoms, the true relation between surface volume ratio and diameter is somewhat deviated from this formulation. Approximately, we apply the following expression:

$$f(d) = a/D - b/D^2 \quad (7)$$

to fit the discrete points in Fig. 3 and show the fitted curves in this figure. We get the fitted results as follows:

$$a = 0.9260 \text{ nm and } b = 0.2348 \text{ nm}^2 \quad \text{for [100] nanowire,}$$

$$a = 0.9522 \text{ nm and } b = 0.4082 \text{ nm}^2 \quad \text{for [110] nanowire,}$$

$$a = 1.0249 \text{ nm and } b = 0.4485 \text{ nm}^2 \quad \text{for [111] nanowire.}$$

We can roughly deduce from these results that the surface thickness δ is $0.66a_0$, $0.68a_0$, and $0.73a_0$ for [100], [110], and [111] nanowires (a_0 is the lattice constant of bulk), respectively. This is in general agreement with the prior simulations on bicrystal³⁸ if we consider that the thickness of bicrystal interface (i.e., $1.6a_0$) is about twice that of surface. These results also imply that surface region approximately consists of two layer atoms.

Once we define unambiguously the surface and core regions, the average stress can be easily calculated under the equilibrium state. The average normal stress along the axial of nanowires can be defined as

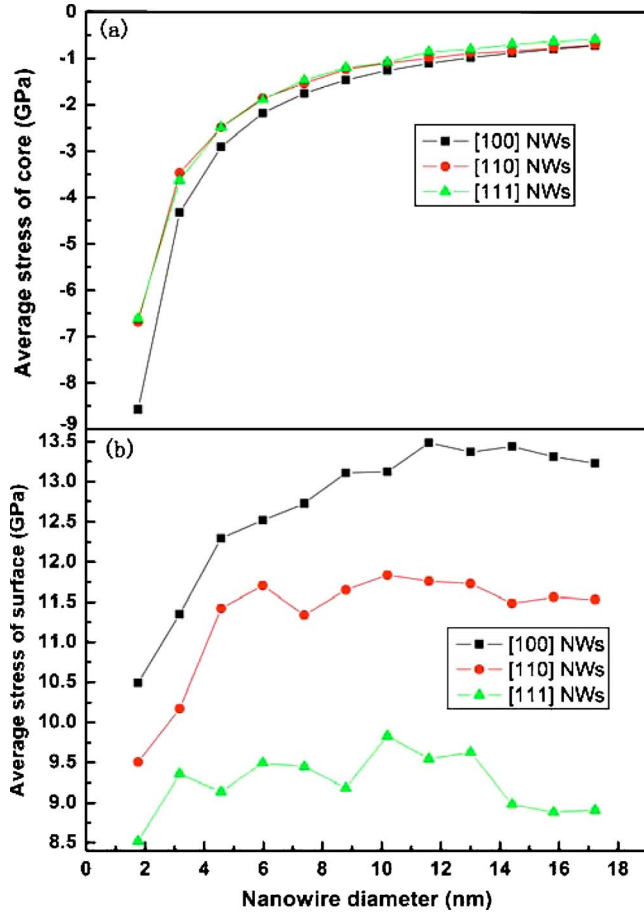


FIG. 4. (Color online) The normal stress along the axial direction as a function of nanowire diameter for (a) core region and (b) surface region.

$$\bar{\sigma}_{xx} = \left(\sum_{i=1}^M \Omega_i \right)^{-1} \left\{ \frac{1}{2} \sum_{i=1}^M \sum_{j=1(j \neq i)}^N F_{ij}^x R_{ij}^x \right\}. \quad (8)$$

For core region, M is the total atomic number of core region, and the summation in the first parentheses is exactly the volume of core region. Similarly, the average stress in surface region can be obtained from Eq. (8) if M is defined as the total atomic number of surface region, and the summed atoms are located in surface region.

Figure 4 shows the average stress of core and surface in nanowires after initial relaxation under the equilibrium state. When the diameter is increased, it can be easily seen that the core stress keeps compressive and decreases gradually to zero, while the surface stress is always tensile and trends to a nonzero constant. If the diameter is large enough to the micrometer scale or above, the core region is essentially stress-free, which is quite different to the case of the surface region. Actually, the surface stress could trend to be a nonzero constant because of the decreasing of coordination. In spite of the nonzero value, the normal stress averaged over the whole cross section is approximately zero.

When comparing the difference of the stress among the three nanowires, we note that the magnitude of the normal stress in both core and surface regions is always largest for

[100] nanowire while the smallest for [111] nanowire. As we know, the compressive stress of core resulted from the contraction of nanowire under surface tensile stress during the initial relaxation. However, the surface stress is closely associated with the number of atomic neighbors and interatomic relative positions. As an example, we calculate the average coordination of these three nanowires with 4.56 nm diameter, and the values are 8.5, 8.64, and 8.73 for [100], [110], and [111] nanowires, respectively. It seems that the lower coordination number results in the higher stress. For these nanowires, the coordination number of surface atoms is far smaller than that of core atoms (i.e., 12), and the symmetrical degree of surface atoms is also much lower than that of core atoms. Due to the broken symmetry and low neighbor number of surface atoms, the surface region presents considerable tensile stress. Because of the contraction of lattice, the average interatomic distance among neighbor atoms in core region is smaller than that in bulk, even though the coordination number of those atoms is still 12. For instance, the average distance of nearest neighbors in core region is $0.7036a_0$, which is evidently lower than $0.7071a_0$ in bulk, so that the core region generally displays the compressive stress.

Further, we may estimate the equilibrium strain in nanowire. In order to deduce the resultant compressive strain in core region, we self-consistently simulate the stress-strain response for nickel bulk by eliminating the surfaces associated with the nanowires. A uniaxial compressive strain is applied along the X axis in the range from 0.0 to -4.0% with a -0.04% increment at each strain step. The periodic boundary conditions are applied in the X , Y , and Z directions under uniaxial loading process. The conjugate gradient method is again employed to determine the energy minimum following each strain step. For metals, it is possible to exhibit nonlinear but elastic behavior, i.e., the stress is essentially nonlinear to strain under the elastic limit.³⁹ In terms of theory of elasticity, the stress can be approximated by Taylor series expansion

$$\sigma = \sigma_0 + c\varepsilon + d\varepsilon^2 + 0(\varepsilon^3) \approx c\varepsilon + d\varepsilon^2, \quad (9)$$

where ε is the strain, and the stress σ_0 is zero in unstrained state. When the strain is small, the fourth term in Eq. (9) may be omitted, so that the stress can be approximately expressed as a quadratic function of strain. We adopt a quadratic-type function to fit the stress-strain curves (see inset picture depicted in Fig. 5) with the framework of the least squares method and present the fitted results as follows:

$$c = 100.42 \text{ GPa and } d = 479.7 \text{ GPa} \text{ for [100] nanowire,}$$

$$c = 173.70 \text{ GPa and } d = -2347.94 \text{ GPa for [110] nanowire,}$$

$$c = 257.56 \text{ GPa and } d = -403.92 \text{ GPa for [111] nanowire,}$$

where c is essentially equal to Young's modulus under unstrained state, and d describes the dependence of Young's modulus on the compressive strain. Evidently, Young's modulus along the [100] direction decreases with compressive strain, while the opposite is true for the [110] and [111] directions. This stress-strain response of bulk is in general

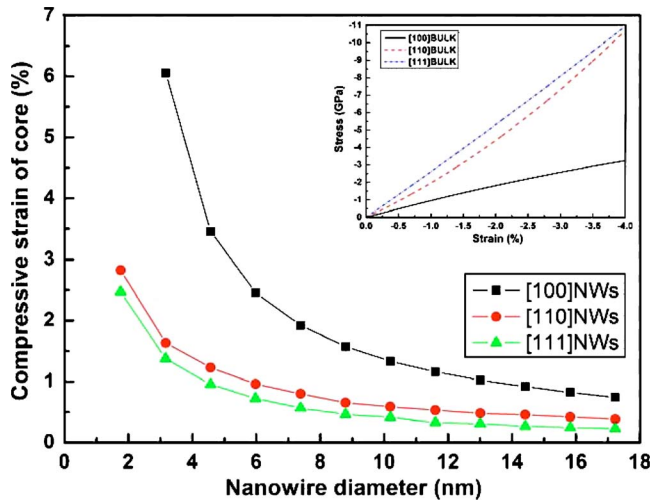


FIG. 5. (Color online) The compressive strain of core as a function of nanowire diameter for three nanowires. (inset) The elastic response of nickel bulk for uniaxial strain applied along [100], [110], and [111] directions under the compressive loading.

agreement with previous *ab initio* or molecular static calculations on strained bulk copper.^{40,41}

According to the elastic response of nickel bulk, we acquire the equilibrium strain of nanowire core (illustrated in Fig. 5) by comparison its stress at equilibrium state with that of the bulk strained along the same orientation to this nanowire. It can be seen that the compressive strain in core region decreases with increasing diameter. This variation is generally consistent with that of the contraction ratio of nanowires depicted in Fig. 2. Evidently, the core of [100] nanowire endures a larger compressive strain than that of [110] and [111] nanowires. This result is closely related to much larger compressive stress of core and smaller modulus in the [100] direction. It is worth noticing that we could not ascertain the equilibrium strain of core for [100] nanowire with 1.76 nm diameter, since the maximum of compressive stress deduced from Eq. (9) is 5.26 GPa, which is remarkably smaller than the compressive stress of core (i.e., 8.56 GPa) calculated from molecular static simulations. However, we may acquire compressive strain of 6.06% for [100] nanowire with 3.16 nm diameter (see Fig. 5) through extrapolating Eq. (9). The compressive strain is lower than 3% for [110] and [111] nanowires considered in our paper. Due to the larger modulus and the smaller core stress (see Fig. 4), these two nanowires endure a much smaller magnitude of equilibrium strain than [100] nanowire. When the diameter increases to 17.23 nm, the equilibrium strain reduces to 0.385% and 0.23% for [110] and [111] nanowires, respectively. This small strain is in good agreement with the results of the contraction ratio (see Fig. 2).

Although we have already obtained the equilibrium strain of core region, it is still very difficult to estimate the corresponding strain of surface region because we are unable to obtain stress-strain response of surface with column area as

presented in our nanowire model, in which surface atoms are not situated in a certain plane, and each atom has different atomic environment. There is no universal response to be suitable for this cylindrical surface with different diameters, whereas it is undoubtedly that the surface endures the tensile strain according to the stress distribution of surface region (see Fig. 4 and inset picture in Fig. 2). The mechanical behaviors, including the elastic and plastic behaviors, are affected greatly by the presence of the equilibrium stress and strain within the nanowire. For example, their existences induce the variations of Young's modulus of nanowires, which have been proved by previous research.¹⁷ How these characteristics under the equilibrium state affect the mechanical behaviors of nanowires is an interesting and challenging work, and requires our further studies.

IV. CONCLUSIONS

In summary, we have employed molecular static approaches with the quantum corrected Sutton-Chen-type many-body force field to investigate the stress and strain characteristics of nickel nanowires with [100], [110], and [111] crystallographic orientations under the equilibrium state. Our studies address the size-dependent effects on these characteristics. We find that the surface tensile stress of the nanowires causes them to contract along the length with respect to bulk fcc lattice and induces the compressive stress in the interior of the nanowires, which is in good agreement with previous simulations on nanowires. With the framework of common neighbor analysis, we divide the nanowire into two regions, surface and core regions, and deduce that surface region approximately consists of two layer atoms. For three orientational nanowires, the surface stress first increases and then trends to a nonzero constant with increasing diameter. Due to the larger surface stress, the core of [100] nanowire is subject to a larger compressive stress than that of [110] and [111] nanowires. Based on the analysis of stress characteristics, we estimate the equilibrium strain of nanowire core through self-consistent comparison with the elastic response of bulk counterpart and show that it decreases with increasing diameter. Owing to much larger compressive stress and smaller modulus in the [100] direction, the core of [100] nanowire endures a larger compressive strain than that of [110] and [111] nanowires. To a certain extent, these size-dependent equilibrium stress and strain could affect the structural stability and some properties of nanowires. These conclusions are summarized from the study of nickel nanowires, but they may be broadened further to other metallic nanowires.

ACKNOWLEDGMENTS

Financial support is provided by the National 973 Project of China (No. 2006CB605102) and the Program for New Century Excellent Talents in Fujian Province University, China (NCETFJ). Y.H.W. is grateful for beneficial discussions with Hui Fang.

*yhwen@xmu.edu.cn

- ¹Y. Kondo and K. Takayanagi, *Science* **289**, 606 (2000).
- ²S. Iijima, L. C. Qin, B. H. Hong, S. C. Bae, S. Y. Youn, and K. S. Kim, *Science* **296**, 611 (2002).
- ³S. Cuenot, C. Fretigny, S. Demoustier-Champagne, and B. Nysten, *Phys. Rev. B* **69**, 165410 (2004).
- ⁴C. Q. Chen, Y. Shi, Y. S. Zhang, J. Zhu, and Y. J. Yan, *Phys. Rev. Lett.* **96**, 075505 (2006).
- ⁵S. G. Nilsson, X. Borriase, and L. Montelius, *Appl. Phys. Lett.* **85**, 3555 (2004).
- ⁶X. Li, T. Ono, Y. Wang, and M. Esashi, *Appl. Phys. Lett.* **83**, 3081 (2003).
- ⁷F. Leonard and A. A. Talin, *Phys. Rev. Lett.* **97**, 026804 (2006).
- ⁸Z. L. Wang, R. P. Gao, Z. W. Pan, and Z. R. Dai, *Adv. Eng. Mater.* **3**, 657 (2001).
- ⁹D. Erts, H. Olin, and J. D. Holmes, *Proc. SPIE* **5123**, 248 (2003).
- ¹⁰E. W. Wong, P. E. Sheehan, and C. M. Lieber, *Science* **277**, 1971 (1997).
- ¹¹B. Wu, A. Heidelberg, and J. J. Boland, *Nat. Mater.* **4**, 525 (2005).
- ¹²D. E. Segall, S. Ismail-Beigi, and T. A. Arias, *Phys. Rev. B* **65**, 214109 (2002).
- ¹³H. Ikeda, Y. Qi, T. Cagin, K. Samwer, W. L. Johnson, and W. A. Goddard, *Phys. Rev. Lett.* **82**, 2900 (1999).
- ¹⁴V. B. Shenoy, *Phys. Rev. B* **71**, 094104 (2005).
- ¹⁵L. G. Zhou and H. Huang, *Appl. Phys. Lett.* **84**, 1940 (2004).
- ¹⁶R. E. Miller and V. B. Shenoy, *Nanotechnology* **11**, 139 (2000).
- ¹⁷H. Liang, M. Upmanyu, and H. Huang, *Phys. Rev. B* **71**, 241403(R) (2005).
- ¹⁸J. Diao, K. Gall, and M. L. Dunn, *Phys. Rev. B* **70**, 075413 (2004).
- ¹⁹W. Liang and M. Zhou, *Nano Lett.* **5**, 2039 (2005).
- ²⁰H. S. Park and C. J. Ji, *Acta Mater.* **54**, 2645 (2006).
- ²¹J. Diao, K. Gall, and M. L. Dunn, *J. Mech. Phys. Solids* **52**, 1935 (2004).
- ²²Y. Kimura, Y. Qi, T. Cagin, and W. A. Goddard (unpublished).
- ²³Y. Qi, T. Cagin, W. L. Johnson, and W. A. Goddard, *J. Chem. Phys.* **115**, 385 (2001).
- ²⁴Y. Qi, Y. T. Cheng, T. Cagin, and W. A. Goddard, *Phys. Rev. B* **66**, 085420 (2002).
- ²⁵S. K. R. S. Sankaranarayanan, V. R. Bhethanabotla, and B. Joseph, *Phys. Rev. B* **71**, 195415 (2005).
- ²⁶A. R. Leach, *Molecular Modelling: Principles and Applications* (Prentice-Hall, London, 2001), p. 253.
- ²⁷M. Parrinello and A. Rahman, *J. Appl. Phys.* **52**, 7182 (1981).
- ²⁸K. S. Cheung and S. Yip, *J. Appl. Phys.* **70**, 5688 (1991).
- ²⁹M. Zhou, *Proc. R. Soc. London, Ser. A* **459**, 2347 (2003).
- ³⁰G. Z. Voronoi, *J. Reine Angew. Math.* **134**, 199 (1908).
- ³¹D. Srolovitz, K. Maeda, V. Vitek, and T. Egami, *Philos. Mag. A* **44**, 847 (1981).
- ³²J. D. Honeycutt and H. C. Andersen, *J. Phys. Chem.* **91**, 4950 (1987).
- ³³H. Jonsson and H. C. Andersen, *Phys. Rev. Lett.* **60**, 2295 (1988).
- ³⁴H. J. Lee, T. Cagin, W. L. Johnson, and W. A. Goddard, *J. Chem. Phys.* **119**, 9858 (2003).
- ³⁵J. Schiotz, F. D. Di Tolla, and K. W. Jacobsen, *Nature (London)* **391**, 561 (1998).
- ³⁶J. Schiotz and K. W. Jacobsen, *Science* **301**, 1357 (2003).
- ³⁷Y. H. Wen, Z. Z. Zhu, R. Z. Zhu, and G. F. Shao, *Physica E (Amsterdam)* **25**, 47 (2004).
- ³⁸S. R. Phillpot, D. Wolf, and H. Gleiter, *J. Appl. Phys.* **78**, 847 (1995).
- ³⁹R. W. Hertzberg, *Deformation and Fracture Mechanics of Engineering Materials* (Wiley, New York, 1983), p. 14.
- ⁴⁰F. Milstein and S. Chantasiriwan, *Phys. Rev. B* **58**, 6006 (1998).
- ⁴¹M. Cerny, M. Sob, J. Pokluda, and P. Sandera, *J. Phys.: Condens. Matter* **16**, 1045 (2004).